# Formulation of the Lateral Boundary Conditions for the NCAR Limited-Area Model

DAVID L. WILLIAMSON AND GERALD L. BROWNING

*National Center for Atmospheric Research,*[1] *Boulder, Colo. 80302*

(Manuscript received 25 June 1973, in revised form 3 October 1973)

ABSTRACT

The Limited-Area Model (LAM) developed at the National Center for Atmospheric Research for use in conjunction with the NCAR Global Circulation Model is described including details of the lateral boundary conditions. One set of experiments is described for which a 2½° global simulation provides the correct or control data against which 2½° LAM forecasts are compared. Three cases are considered in which the LAM inflow boundary values are provided by the 2½° global forecast, a 5° global forecast, or are held fixed equal to the initial values. Forecasts produced by the LAM with finer grids (up to ⅝°) are also shown. Although based on simulated data, the results indicate that the Limited-Area Model shows good potential for short-range forecasting.

## 1. Introduction

The necessity for a fine-grid structure to adequately resolve the small-scale features of the atmosphere is well known. However, with the present computers and advanced baroclinic equation models it is impractical to use such fine grids over the entire spherical earth or even over a hemisphere. Because of these limitations, there has been increased interest in the use of a fine mesh limited to some smaller region, say the continental United States, where boundary conditions must be applied on the edges of the forecast region. The boundaries of the region are generally not physical boundaries such as coastlines of oceans so that the boundary conditions cannot be solely derived from physical constraints on the flow such as zero normal velocity.

Several investigators have obtained boundary conditions for a limited-area model from a parallel integration of the model over a coarser grid covering a larger area. Birchfield (1960) used a moving fine mesh imbedded in a coarse mesh to forecast hurricane movement with the barotropic vorticity equation. Hill (1968) integrated a two-level baroclinic model over a series of nested grids with successively smaller domains and grid intervals so that the final grid size was as small as desired. Wang and Halpern (1970) obtained boundary conditions for a limited-area barotropic primitive equation model from a coarse-mesh hemispheric model. Both Hill, and Wang and Halpern obtained boundary data for all the prognostic variables of the limited-area fine-mesh models by interpolation of the data produced by the coarse-mesh integration. As a result, both studies noted the generation of small-scale spatial oscillations in the interior solution and attributed these oscillations to the boundary conditions.

Shapiro and O'Brien (1970) studied a method which eliminates these instabilities in the barotropic vorticity equation. Their method, following Charney *et al.* (1950), did not specify all variables on the boundary, but rather computed the vorticity on outflow boundaries by a pseudo-Lagrangian scheme and specified the vorticity on the inflow boundary. This scheme effectively eliminated the numerical instabilities associated with specifying the vorticity on both inflow and outflow boundaries. Asselin (1972) integrated a limited-area primitive equation barotropic model with boundary conditions obtained from a hemispheric coarse-mesh model. On the boundary, he specified the normal velocity everywhere and the absolute vorticity at points of inflow. At points of outflow, he computed the absolute vorticity by Lagrangian advection. He found that these boundary conditions generated only a very small amount of noise.

In a recent theoretical study, Oliger and Sundström (1973) concluded that the initial boundary value problem for the nonviscous baroclinic primitive equations is ill-posed for any specification of the boundary conditions along the lateral boundaries. When the boundary conditions are overspecified, a smooth solution does not exist; and when they are underspecified, there is no unique solution. These difficulties are due to the hydrostatic approximation in the baroclinic primitive equations and do not occur in the initial boundary-value problem for the Eulerian equations of motion without the hydrostatic assumption (Serrin, 1959). Oliger and Sundström also showed that this difficulty can be

[1] The National Center for Atmospheric Research is sponsored by the National Science Foundation.

eliminated in the baroclinic primitive equations by the addition of a suitable viscosity term.

At NCAR we have developed a Limited-Area Model (LAM) to be used in conjunction with the Global Circulation Model (GCM). The physical basis of the LAM is identical to that of the GCM; the only difference between the two models is the horizontal domain and grid interval. The basic approximations involved in the GCM, and thus in the LAM, are described by Kasahara and Washington (1967, 1971) and Washington and Kasahara (1970), and the finite-difference approximations by Oliger *et al.* (1970). The boundary conditions used for the LAM are described in the following section. In Section 3, we present some results of preliminary tests of the LAM using simulated data.

## 2. Lateral boundary conditions

We assume that the prognostic and diagnostic variables are known at all spatial grid points at times $(\tau-1)\Delta t$ and $\tau\Delta t$. We then compute the prognostic variables at time $(\tau+1)\Delta t$. Since the GCM finite-difference operators involve only grid points immediately adjacent to the one at which the forecast is being made, these operators can be applied to compute the prognostic variables at time $(\tau+1)\Delta t$ everywhere except at grid points on the boundary. The prognostic variables are determined at time $(\tau+1)\Delta t$ on the boundary by one of two methods depending on the direction of the winds computed by the global model. If the winds computed by the global model (referred to as global winds) on the LAM boundary are directed into the LAM domain, the LAM prognostic variables are determined from the corresponding global model variables by linear interpolation in the space-time plane of the boundary. If the global winds on the LAM boundary are directed out of the LAM domain, the LAM prognostic variables are determined by an extrapolation from the LAM interior to the boundary. This extrapolation is simply the horizontal advection of LAM variables by the global wind as done by Shapiro and O'Brien (1970) with the vorticity.

The extrapolation is made cumbersome by the details of the NCAR GCM and LAM grids which are staggered in time. Essentially, we determine the path that an air parcel would follow if it were subject only to advection by the global wind at the boundary. This path is a space-time line through the boundary point which intersects a space-time plane on which the prognostic variables are known. The values of the prognostic variables are obtained at this intersection by interpolation, and the LAM boundary values are set equal to these interpolated values.

We give the interpolation formulas for a general boundary point $(i,j)$ whose longitude is $\lambda_i$ and latitude is $\theta_j$ (Fig. 1). The interpolation is over one of the four triangles shown in the figure depending on the location of the interior with respect to the point and on the direction of the global wind. We give the general form of the interpolation which can be made specific when applied to a particular case. As mentioned earlier, the LAM grid is staggered in time so that at any one time the variables are defined at every other grid point. In Fig. 1 the grid points represented by ×'s have values at time $\tau(\Delta t)$ and those by dots have values at $(\tau-1)\Delta t$ and $(\tau+1)\Delta t$. We need to determine the prognostic variables at the general boundary point $(i,j)$ at $(\tau+1)\Delta t$.

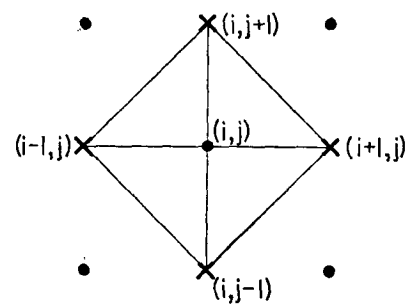


FIG. 1. Indices related to a general grid point. The ×'s are grid points with data at time $\tau\Delta t$ and the dots are points with data at $(\tau-1)\Delta t$ and $(\tau+1)\Delta t$.

Let $U$ and $V$ be the interpolated global velocity values at the point $(i,j)$ at time $(\tau+1)\Delta t$. We assume that $U$ and $V$ are nonzero. The equation of the line through the points

$$[\lambda_i,\ \theta_j,\ (\tau+1)\Delta t]$$

and

$$\left[\lambda_i-\frac{U\Delta t}{a\cos\theta_j},\ \theta_j-\frac{V\Delta t}{a},\ \tau\Delta t\right]$$

is

$$\frac{\lambda-\lambda_i}{\dfrac{U\Delta t}{a\cos\theta_j}}=\frac{\theta-\theta_j}{\dfrac{V\Delta t}{a}}=\frac{t-(\tau+1)\Delta t}{-\Delta t}, \tag{1}$$

or

$$(\theta-\theta_j)=(\lambda-\lambda_i)\frac{V\cos\theta_j}{U}, \tag{1a}$$

$$t-(\tau+1)\Delta t=(\lambda-\lambda_i)\frac{a\cos\theta_j}{U}. \tag{1b}$$

The line given by Eqs. (1) is essentially the path in space and time along which the air parcel is assumed to move. We need to interpolate the prognostic variables at the point where this line intersects the triangle (Fig. 1) of the quadrant from which the global wind is directed; for example, if $U<0$ and $V<0$, the triangle is defined by the points $(i,j)$, $(i+1,\ j)$, $(i,\ j+1)$. Since the center point $(i,j)$ is not at the same time level as the closest surrounding points, the triangle lies on a space-time plane.

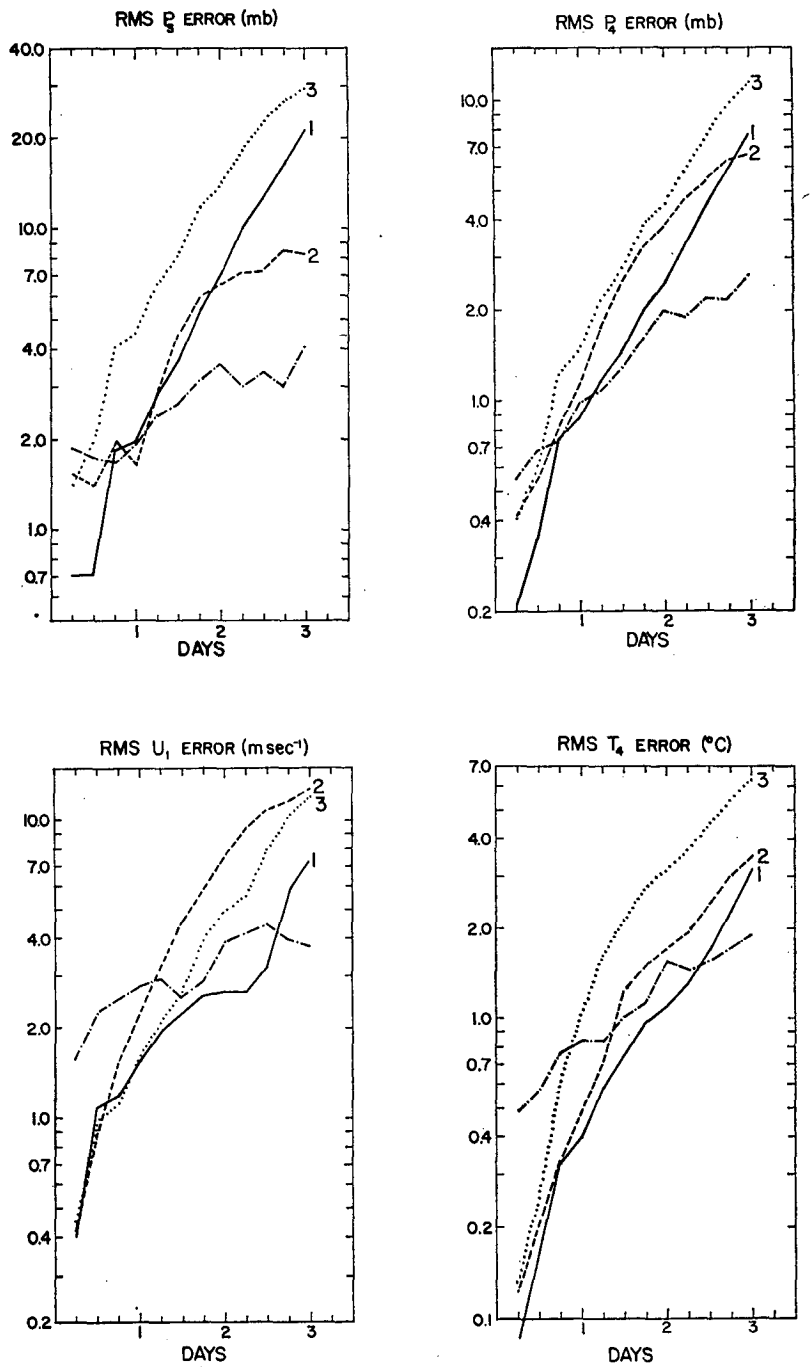


FIG. 2. Root-mean-square $P_s$, $u_1$, $P_4$, $T_4$ errors resulting from: (1) $2\frac{1}{2}°$ LAM with inflow boundary condition from $2\frac{1}{2}°$ model, (2) $2\frac{1}{2}°$ LAM with inflow boundary conditions from 5° model and (3) $2\frac{1}{2}°$ LAM with constant inflow boundary conditions equal to initial values. The dash-dot line is the error of the 5° global as compared to the $2\frac{1}{2}°$ global.

The equation of the plane through $(i, j, \tau-1)$ and the two points $(i-\mathrm{sgn}U, j, \tau)$ and $(i, j-\mathrm{sgn}V, \tau)$ is

$$(\mathrm{sgn}V)\frac{\Delta t}{\Delta\theta}(\theta-\theta_j)+(\mathrm{sgn}U)\frac{\Delta t}{\Delta\lambda}(\lambda-\lambda_i)+t-(\tau-1)\Delta t=0, \quad (2)$$

where

$$\mathrm{sgn}U=\begin{cases}+1, & \text{if } U>0\\ -1, & \text{if } U<0\end{cases}$$

Similarly for $V$.

The intersection of the plane and line is then obtained from (1) and (2) as

$$(\lambda-\lambda_i)=-2\Delta t\left[\frac{a\cos\theta_j}{U}+(\operatorname{sgn}U)\frac{\Delta t}{\Delta\lambda}+(\operatorname{sgn}V)\frac{\Delta t}{\Delta\theta}\frac{V\cos\theta_j}{U}\right]^{-1}, \quad (3a)$$

$$(\theta-\theta_j)=-2\Delta t\left[\frac{a}{V}+(\operatorname{sgn}U)\frac{\Delta t}{\Delta\lambda}\frac{U}{V\cos\theta_j}+(\operatorname{sgn}V)\frac{\Delta t}{\Delta\theta}\right]^{-1}. \quad (3b)$$

For the interpolation over the triangle of some field $\psi$, we assume a linear variation given by

$$\psi(\lambda,\theta)=\psi_{ij}^{\tau-1}+(\operatorname{sgn}U)\frac{\psi_{ij}^{\tau-1}-\psi_{i-\operatorname{sgn}U,j}^{\tau}}{\Delta\lambda}(\lambda-\lambda_i)+(\operatorname{sgn}V)\frac{\psi_{ij}^{\tau-1}-\psi_{i,j-\operatorname{sgn}V}^{\tau}}{\Delta\theta}(\theta-\theta_j). \quad (4)$$

The boundary value is then given by (4) with $\lambda$ and $\theta$ determined by (3).

## 3. Tests with simulated data

In this section, we present experiments with simulated data designed to test the LAM. In early experiments, we noted two-grid-interval noise propagating into the interior of the LAM domain from the boundaries. Although this noise did not grow to dominating amplitudes in forecasts of several days, we increased the damping moderately near the boundaries to reduce it. The horizontal viscosity coefficient and pressure smoothing coefficient were increased by a factor of 4 in the 5° band adjacent to the boundary and by a factor of 2 at the next interior 5° band. Elsewhere, the values were the same as used in the global model. This extra smoothing had very little effect on the fields.

We performed one series of experiments to investigate the effect of the lateral boundary conditions on the LAM solution. To do this, we took a three-day period from a standard 2½° global simulation as the control data. We then ran several 2½° LAM cases starting from the control data and compared the 2½° LAM forecasts with the standard 2½° global case. The only differences in the LAM cases are the inflow boundary conditions. In the first case, the inflow boundary conditions are taken directly from the standard 2½° global case and are thus correct. The only error in this LAM integration is produced by the outflow boundary conditions. In the second case, the inflow boundary conditions are determined from a 5° global forecast over the same period. Compared to the first case, this LAM case has an additional error in the inflow boundary conditions since the 5° global model produces a different forecast compared to the 2½° global standard case. In the third case, the inflow boundary conditions are held fixed in time equal to the initial values of the first case.

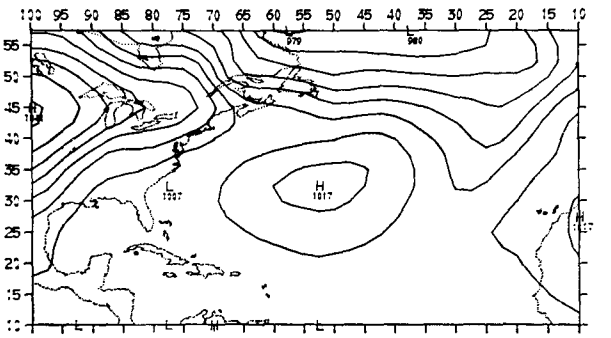

FIG. 3. Initial surface pressure distribution for the 2½° LAM forecasts: contour interval, 5 mb.

Root-mean-square (rms) errors (differences between the LAM cases and the standard 2½° global case) taken over the 5° grid subset of the 2½° LAM mesh are shown in Fig. 2 for surface pressure ($P_s$), pressure at 12 km ($P_4$), zonal wind at 1.5 km ($u_1$), and temperature at 10.5 km ($T_4$). $P_s$, $P_4$ and $T_4$ were chosen since they exhibit the type of error accumulation observed in most of the variables, while $u_1$ is shown for its exceptional behavior as discussed below. The numbered curves refer to the first, second and third LAM cases; the rms error is computed over the interior of the LAM domain which has no extra smoothing. For most fields, the error from Case 1 is less than that from Case 2 which, in turn, is less than that of Case 3. This relation implies that there is a slight gain by using the 5° global model to specify the inflow boundary conditions over holding the boundary conditions fixed in time. However, the errors from the 5° global boundary conditions degrade slightly the interior solution of most variables compared to the solution using inflow boundary conditions with no error. This relation does not hold for all fields, though, as is seen in the graph of $u_1$ error. Thus, for some fields the constant boundary conditions result in a smaller rms error.

The additional curve (dash-dot) plotted in Fig. 2 is the rms error of the 5° global compared to the 2½° global over the interior of the LAM domain. In most fields, the rms error of all the LAM cases exceeds the error of the 5° global case after two days and in many fields after one day. The predictability error growth of the 2½° model is much slower than the error accumulation of the 5° model vs 2½° model data (Williamson, 1973). Thus, the error accumulation in Fig. 2 of the 2½° LAM cases vs the 2½° global model is not a predictability error growth but rather an accumulation of boundary errors propagating into the interior of the LAM domain resulting from the ill-posed property of

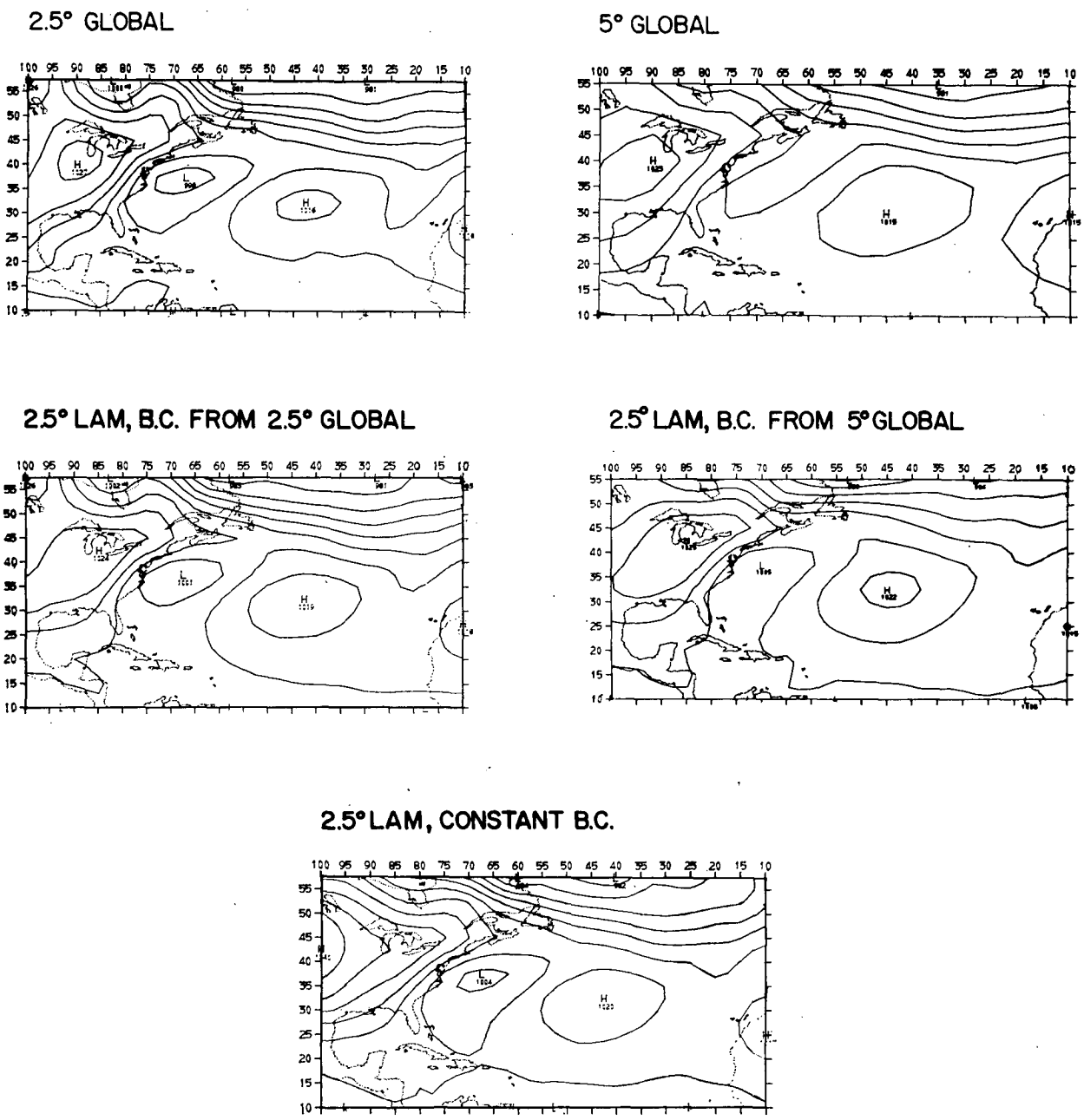


FIG. 4. One-day surface pressure forecasts: contour interval, 5 mb. The figures are copied directly from the graphical computer output. A 5-point smoothing operator with a small coefficient was applied during the processing.

the inviscid boundary value problem. If the rms error represents a measure of the forecast quality, Fig. 2 would imply that the LAM is useful for only a period of a day or so. However, the rms values of the LAM forecasts might be large due to small-scale noise caused by the boundary conditions in the LAM. The forecasts of the larger scale features might be better than the rms errors indicate. In addition, these LAM forecasts are with a grid interval of only $2\frac{1}{2}°$. In practice, one would use a much finer mesh interval for the LAM which would result in a larger improvement of wave amplitudes and phase speeds in the LAM. Unfortunately, at present we are not able to run a global model with grid size less than $2\frac{1}{2}°$ to provide a standard case.

Fig. 3 shows the initial surface pressure distribution used in all the above cases. Fig. 4 depicts the forecast of surface pressure after one day. The upper left frame is the standard $2\frac{1}{2}°$ global case. The low originally off the

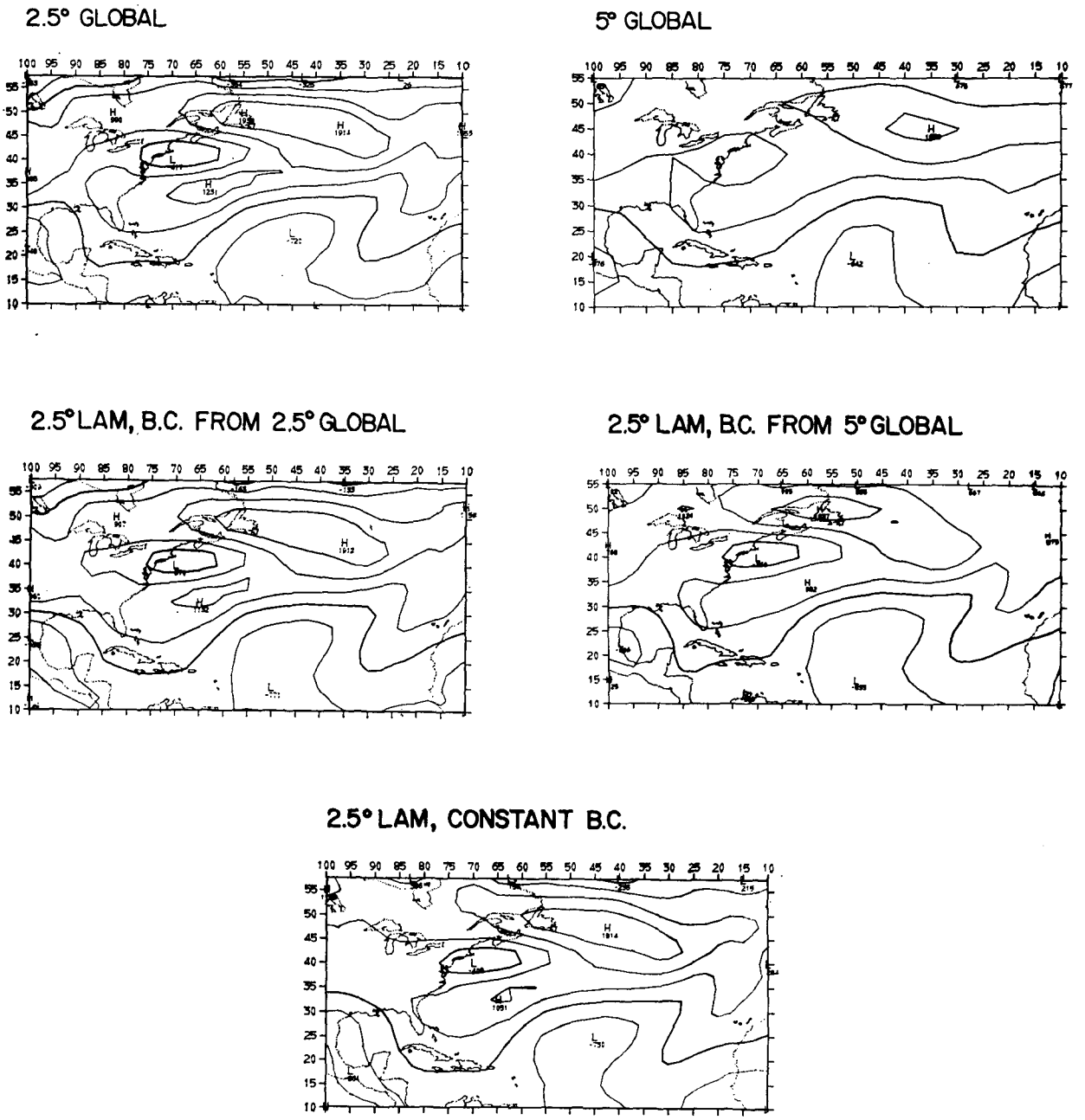


FIG. 5. One-day forecast of the zonal wind at 1.5 km: contour interval, 5 m sec$^{-1}$. The darker contour is the zero contour (see Fig. 4 legend).

southeastern coast of the United States moved northeast and deepened by about 10 mb while the high originally on the western boundary of the LAM moved eastward to an area south of the Great Lakes. The top right frame shows the 5° global forecast. In this case, the low appears only as a weak trough and the high, while moving to the right location, loses some of its intensity. The lower three frames of the figure show the three LAM cases. All three cases retain the low better than the 5° global, with Case 1 the best and Case 3 slightly better than Case 2. However, Case 3 shows the effects of the fixed boundary conditions in the position of the high originally on the western boundary. In this case, the high does not move off the boundary, whereas in all other cases it moves eastward, as it should.

Fig. 5 shows the one-day forecast of zonal wind at 1.5 km ($u_1$) for the same cases as Fig. 4. If we compare the $2\frac{1}{2}°$ LAM cases and the 5° global cases, the larger scale features of the $2\frac{1}{2}°$ LAM cases are more like the control case. The large positive area in the North

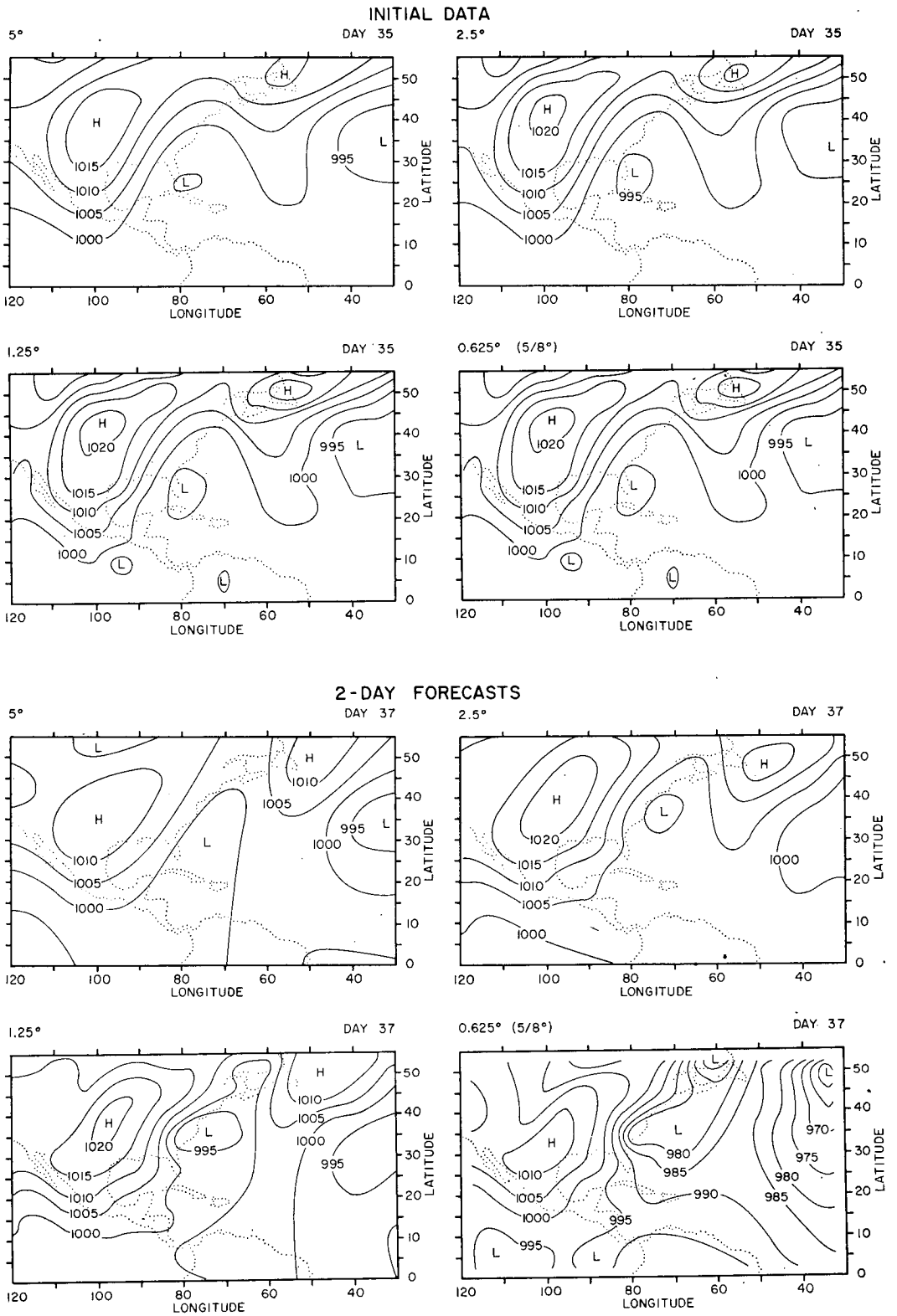


FIG. 6. Initial and two-day forecasts of surface pressure with a 5° global model and $2\frac{1}{2}°$, $1\frac{1}{4}°$ and $\frac{5}{8}°$ Limited-Area Models. The contours were slightly smoothed in drafting.

Atlantic, however, is distorted more in Case 2 than in 1 and 3. This feature might account for the rms $u_1$ error of Case 2 being greater than that of Case 3 in Fig. 2. Figs. 4 and 5 suggest that the larger scale features are handled better by the LAM than by the global model with coarser resolution.

We have carried out several additional experiments using simulated data with LAM's having mesh intervals $<2\frac{1}{2}°$. The boundary conditions used are those described in Section 2. In these cases, we have no control or correct case to compare and thus can only examine the forecasts subjectively. Fig. 6 shows the initial surface pressure for one set of experiments with a 5° global and $2\frac{1}{2}°$, $1\frac{1}{4}°$ and $\frac{5}{8}°$ LAM's. The LAM initial states were obtained from the 5° global case using cubic-spline interpolation and hence contain no meteorologically significant features with scales finer than those of the 5° global. Fig. 6 also shows the two-day forecasts of surface pressure. Notice that the higher-resolution LAM's retain the high and low amplitudes better and move the systems faster. This indicates that the finer-resolution LAM's tend to reduce the amplitude and phase errors present in the coarse 5° global model.

Fig. 7 shows the surface pressure for another two-day forecast starting from simulated data using the $1\frac{1}{4}°$ LAM with the 5° global providing the boundary conditions. Again, the amplitudes of the systems and the phase speeds are greater in the LAM. Fig. 7, which is copied directly from graphical computer output with no additional smoothing, shows the amount of noise introduced by the boundary conditions in this case.

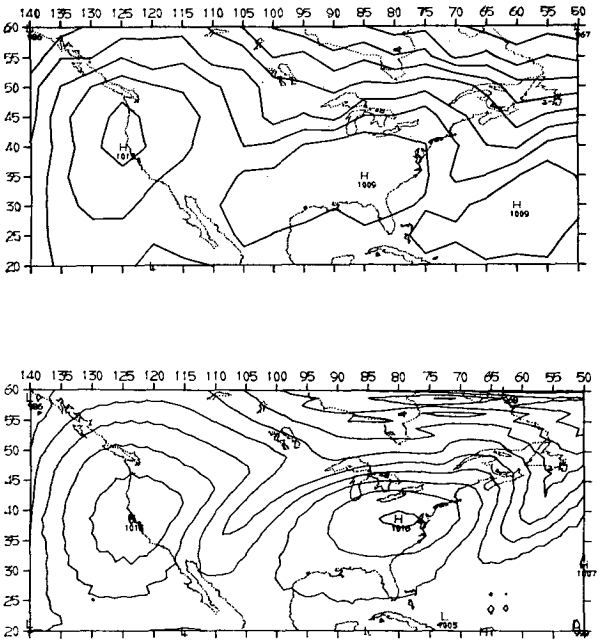

FIG. 7. Two-day forecast of surface pressure by a 5° global model (upper) and a $1\frac{1}{4}°$ Limited-Area Model (lower): contour interval, 5 mb. The figures are copied directly from the graphical computer output without smoothing.

## 4. Conclusions

The NCAR Limited-Area Model is described along with details of the necessary lateral boundary conditions. For the first set of experiments described, a $2\frac{1}{2}°$ global simulation provides the control data against which $2\frac{1}{2}°$ LAM's are compared. The LAM inflow boundary conditions are provided by the $2\frac{1}{2}°$ global forecast, a 5° global forecast, or are held fixed equal to the initial values. The rms errors show that for many fields, but not all, the 5° global boundary conditions do provide a better forecast than the fixed boundary conditions. A slightly better forecast could be obtained by using more accurate inflow values; however, a significant error would still remain due to the outflow boundary conditions. The rms errors indicate that the LAM offers good potential for short-range forecasts of a period of a day or two.

Subjective examination of the forecasts produced by the LAM with finer grids (up to $\frac{5}{8}°$) shows that the finer-mesh models forecast with less amplitude and phase errors than the coarser (5°) global models for a period of a few days.

It should be pointed out that the experiments reported here are a first test of the usefulness of the LAM. All cases are based on simulated data, wherein the initial states for the finer-resolution LAM's are obtained by interpolation and thus do not contain meteorologically significant small-scale features. The ultimate test of the LAM will come when it is used to forecast real atmospheric situations. Such tests are currently being initiated at NCAR.

*Acknowledgments.* This work was initiated several years ago in collaboration with Warren Washington; we are grateful for his participation. We also thank Akira Kasahara and Warren Washington for helpful comments on the original manuscript and Ann Lundberg for editorial assistance and typing the manuscript. The major processing program was written by David Kennison with auxiliary processors by John Donnelly; Judith Slater and Gloria Williamson supervised the running of the model.

REFERENCES

Asselin, R., 1972: Integration of a semi-implicit model with time-dependent boundary conditions. *Atmosphere*, **10**, 44–55.

Birchfield, G. E., 1960: Numerical prediction of hurricane movement with the use of a fine grid. *J. Meteor.*, **17**, 406–414.

Charney, J. G., R. Fjortøft and J. von Neumann, 1950: Numerical integration of the barotropic vorticity equation. *Tellus*, **2**, 237–254.

Hill, G. E., 1968: Grid telescoping in numerical weather prediction. *J. Appl. Meteor.*, **7**, 29–38.

Kasahara, A., and W. M. Washington, 1967: NCAR global general circulation model of the atmosphere. *Mon. Wea. Rev.*, **95**, 389–402.

——, and ——, 1971: General circulation experiments with a six-layer NCAR model including orography, cloudiness and surface temperature calculations. *J. Atmos. Sci.*, **28**, 657–701.

Oliger, J. E., R. E. Wellck, A. Kasahara and W. M. Washington, 1970: Description of the NCAR Global Circulation Model. NCAR TN-56, 94 pp.

—— and A. Sundström, 1973: Theoretical and practical problems in formulating boundary conditions for a limited-area model (in preparation).

Serrin, J., 1959: On the uniqueness of compressible fluid motions. *Arch. Rat. Mech. Anal.*, **3**, 271–288.

Shapiro, M. A., and J. J. O'Brien, 1970: Boundary conditions for fine-mesh limited-area forecasts. *J. Appl. Meteor.*, **9**, 345–349.

Wang, H.-H., and P. Halpern, 1970: Experiments with a regional fine-mesh prediction model. *J. Appl. Meteor.*, **9**, 545–553.

Washington, W. M., and A. Kasahara, 1970: A January simulation experiment with the two-layer version of the NCAR global circulation model. *Mon. Wea. Rev.*, **98**, 559–580.

Williamson, D. L., 1973: The effect of forecast error accumulation on four-dimensional data assimilation. *J. Atmos. Sci.*, **30**, 537–543.